Rotation-aligned isomer and oblate collectivity in ^{196}Pt

S. G. Wahid,[1] S. K. Tandel,[1,2,*] P. Chowdhury,[2] R. V. F. Janssens,[3] M. P. Carpenter,[3] T. L. Khoo,[3] F. G. Kondev,[3] T. Lauritsen,[3] C. J. Lister,[2,3] D. Seweryniak,[3] and S. Zhu[3]

[1]*UM-DAE Centre for Excellence in Basic Sciences, Mumbai 400098, India*

[2]*Department of Physics, University of Massachusetts Lowell, Lowell, Massachusetts 01854, USA*

[3]*Argonne National Laboratory, Argonne, Illinois 60439, USA*

(Received 12 June 2015; revised manuscript received 10 October 2015; published 25 November 2015)

An oblate rotational sequence, built on an aligned, two-quasineutron isomeric state has been established in ^{196}Pt. The isomer has a half-life of 7.7(7) ns and is associated with the $I^{\pi} = 12^{+}$, $(i_{13/2})^2$ neutron configuration. Excited states, with angular momentum generated primarily through successive nucleon alignments, have been populated through $1p$ transfer from ^{197}Au. The nucleus ^{196}Pt is the most neutron-rich Pt isotope for which high-spin states, beyond the 12^{+} isomeric state, have been established thus far. Cranked shell model calculations have been performed to understand shape evolution with spin, and the role of nucleons occupying specific Nilsson orbitals in generating aligned angular momentum for both prolate and oblate deformations has been explored.

DOI: 10.1103/PhysRevC.92.054323 PACS number(s): 21.10.Re, 21.60.Ev, 23.20.Lv, 27.80.+w

I. INTRODUCTION

The region of neutron-rich, $A \approx 190$ nuclei, approaching doubly magic ^{208}Pb, is characterized by diverse structure phenomena. While collectivity diminishes with increasing neutron number, oblate rotation-aligned states tend to be favored at high spin over prolate excitations, in isotopes of Hf ($Z = 72$) to Hg ($Z = 80$) [1–4]. Substantial high-spin information is available for lighter Pt isotopes [2,5] which are accessible through heavy-ion fusion evaporation reactions. Isotopes of Pt ($Z = 78$), beginning with ^{196}Pt, can be reached only through either inelastic excitation, multinucleon transfer, or projectile fragmentation reactions [6,7]. Consequently, these isotopes are not as well studied as the lighter ones. These nuclei are particularly interesting to explore since oblate shapes are predicted to be more favored. Furthermore, due to their transitional nature, both collective and intrinsic degrees of freedom may play an important role in determining the excited level structure.

The region of proton-rich Pt isotopes is characterized by substantial ground-state deformation that decreases in magnitude for the neutron-rich nuclei, due primarily to the presence of the $N = 126$ spherical shell gap. Gamma softness in varying degrees is a feature common to all Pt isotopes owing to the relatively small number of valence nucleons. For the doubly even Pt isotopes, a rather sudden change in the energy sequence of the yrast, positive-parity, structure is evident around 10–12 $\hbar$ in $^{188-194}$Pt [2,5]. In fact, the 12^{+} state is isomeric, and the rotational sequence built on this level is characterized by a moment of inertia much larger than that of the ground-state band. The observations have been interpreted in terms of a rotation-aligned structure built on two quasineutrons occupying the $i_{13/2}$ orbital. The maximal alignment of the intrinsic angular momentum of the two $i_{13/2}$ quasineutrons generates the 12^{+} state. Subsequent g-factor measurements have confirmed the neutron character of this 12^{+} level [8].

Transition energies in the sequence built on the 12^{+} state in the lighter Pt nuclei, up to ^{192}Pt [5], exhibit the usual smooth increase with spin, as expected for a rotational band. In ^{194}Pt, this sequence is less regular, and the observation is attributed to decreased collectivity [9]. The measured half-lives for the 12^{+} isomeric states exhibit a small, but gradual increase with neutron number from ^{188}Pt to ^{194}Pt. Excited states in ^{196}Pt had been studied through Coulomb excitation with a ^{208}Pb beam [10]. Levels up to 8^{+} had been identified, and a 10^{+} state was tentatively proposed. The observed level structure and its interpretation in terms of various theoretical models implied the presence of both triaxiality and γ softness [10]. Considerable experimental and theoretical effort has been focused on understanding the shapes of Pt isotopes [11–15]. Proton-rich isotopes exhibit a prolate energy minimum near the ground state, while a preference for triaxial to oblate shapes is visible with increase in neutron number. The primary objective in the present work was to identify positive-parity, yrast states at high spin and to search for the 12^{+} isomer, in order to study the evolution of both collectivity and oblate rotation-aligned states with increasing neutron number, as well as nucleon alignments and their role in generating angular momentum.

II. EXPERIMENT AND DATA ANALYSIS

Excited states in ^{196}Pt were populated through $1p$ transfer from ^{197}Au, with a 1450-MeV ^{209}Bi beam incident on a thick, 50 mg/cm^2 Au foil. Various Pt isotopes, ranging from $^{188-198}$Pt, were populated through multinucleon transfer reactions between the ^{209}Bi beam and the ^{197}Au target. The present work is focused on ^{196}Pt, and the detailed results and interpretation are outlined. A summary of new information on even-Pt isotopes ranging from $A = 192$–198, and the evolution of collectivity at high spin in the Pt isotopic chain, is published elsewhere [16]. The Gammasphere array [17,18], which was comprised of 100 Compton-suppressed Ge detectors for this

*Corresponding author: sujit.tandel@cbs.ac.in

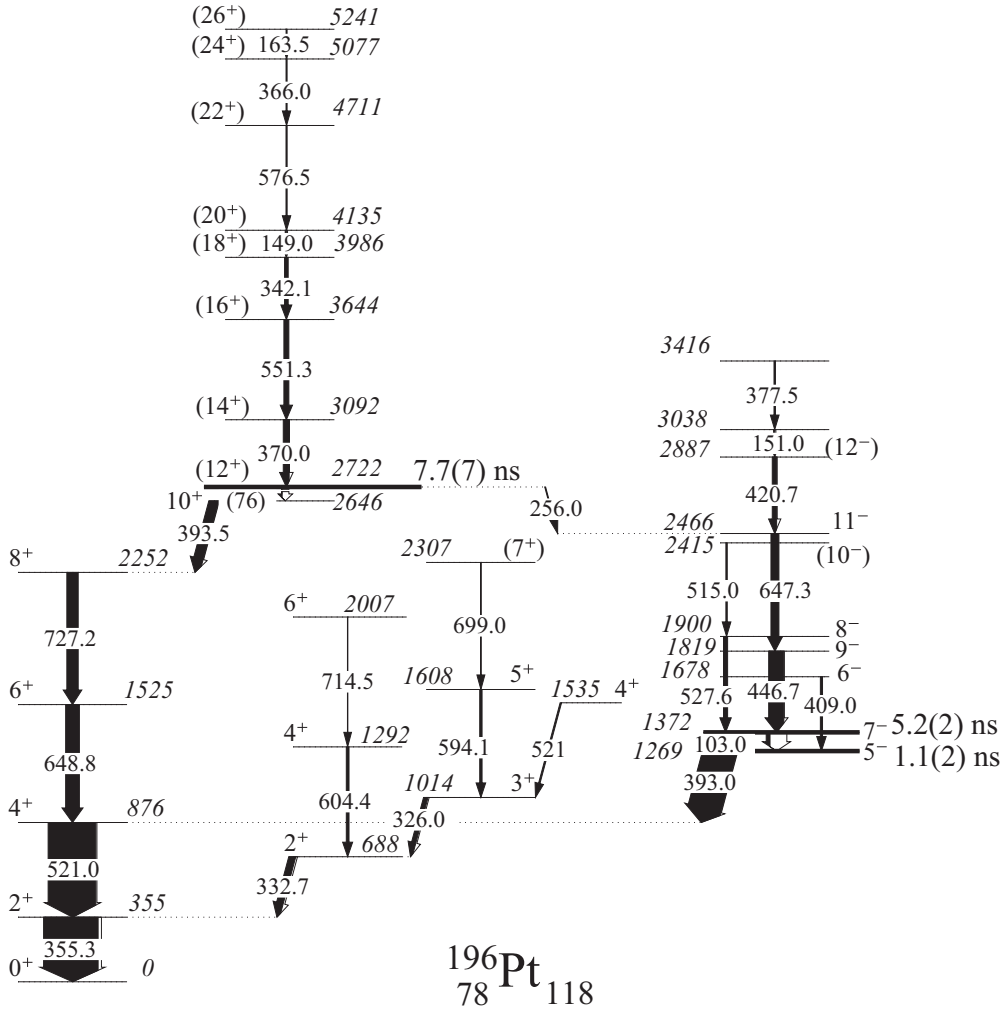

FIG. 1. Partial decay scheme for ^{196}Pt illustrating transitions observed in the present work. Transitions above the 8^+ level in the positive parity band, including the isomeric 12^+ state, are newly established, as are a number of negative-parity levels.

experiment, was used to record three- or higher-fold γ-ray coincidence events. The ^{209}Bi beam, with the natural 82.5 ns pulsing from ATLAS, was incident on the target for $\approx$1 ns, but was then swept away for a 825-ns off period. This enabled the recording of prompt and delayed coincidence events as well as the measurement of half-lives ranging from a few to several hundred ns.

The raw data were sorted into three- and four-dimensional symmetric γ-ray energy histograms and analyzed using the RADWARE suite of programs [19]. To isolate prompt coincidence events, three- and four-dimensional histograms, consisting of γ rays detected within $\pm$20 ns and $\pm$40 ns of the trigger, were inspected. Wider time cuts were employed to investigate coincidence relationships across isomeric states. While most of the double-gated spectra were free of contaminant transitions, in some cases triple-gated spectra proved beneficial to resolve ambiguities and confirm the placement of various transitions.

For determining the multipolarity of transitions of interest, the method of directional angular correlations from oriented nuclei (DCO) [20,21] was utilized. For this purpose, a matrix was constructed with γ rays detected at $90^\circ \pm 10^\circ$ with respect to the beam direction on one axis, and those detected at $30^\circ/150^\circ \pm 10^\circ$ on the other. The experimental DCO ratio $R_{\rm DCO}(\gamma)$ of a γ transition is then determined as

$$R_{\rm DCO}(\gamma) = \frac{I_\gamma\ (30^\circ/150^\circ,\ 90^\circ)}{I_\gamma\ (90^\circ,\ 30^\circ/150^\circ)}\ , \qquad (1)$$

where $I_\gamma\ (\theta_1, \theta_2)$ is the intensity of the γ transition observed at the angle θ_1, in coincidence with a stretched-$E2$ transition observed at θ_2. While the applicability of the DCO technique to inelastic and transfer reactions is limited in comparison to what can be obtained following fusion evaporation, its reliability in the present case was demonstrated from an analysis of transitions of known multipolarity, unless a long-lived state separates the γ rays of interest.

Histograms of the time difference between transitions feeding and de-exciting isomeric states were generated using the TSCAN [22] software package. Half-lives ranging from $\approx$2–10 ns were determined. In general, the centroid of the time-difference spectrum of γ rays across a long-lived state is shifted when compared to that for two prompt transitions (with similar energies), by an amount equal to the mean life of the isomer. While it is more common to inspect the time distributions of individual γ rays and compare these with the

ones measured for prompt transitions of similar energy in order to extract the mean life, this technique was not employed here due to the large number of nuclei populated in this experiment, and the contamination these induce in spectra. The applicability of the method was tested for several known short-lived (ns) isomers in various Pt and Hg isotopes. In all cases, half-lives determined from the present analysis were in agreement with the adopted values.

III. RESULTS

The nucleus ^{196}Pt had been studied earlier through Coulomb excitation and levels up to 8^+ in the ground-state band had been established, with a 10^+ state tentatively placed as well [10]. In addition, levels up to spin $8\hbar$ built on the second 2^+ excited state, and up to 9^- in a negative-parity sequence, were previously identified. In the present work, the decay scheme for ^{196}Pt has been expanded with the addition of 14 new transitions. The resulting level scheme can be found in Fig. 1. Table I summarizes the information obtained for all ^{196}Pt transitions. Eight of these are placed above the 8^+ level in the ground-state band (Fig. 1). These transitions are in coincidence with each other and are, therefore, placed in a cascade ordered according to decreasing total intensity. The transitions in the positive-parity yrast sequence are displayed in Figs. 2(a) and (b), which are triple-γ coincidence spectra with gates placed on the 355- and 727-keV, and 649- and 727-keV transitions, respectively, in the ground-state band. The 76.5-keV, $(12^+) \rightarrow 10^+$ transition is not directly observed, primarily due to strong contamination from Au (target) x rays in the region of interest, and partly due to the large internal conversion coefficient and reduced detection efficiency at this low energy. However, its placement is substantiated through the unambiguous observation of the 256-keV, $(12^+) \rightarrow 11^-$ transition (Fig. 1) linking the positive- and negative-parity sequences. This 256-keV transition is clearly visible in coincidence with transitions below the 11^- level and above the (12^+) state. But it is not in coincidence with either the 727.2-keV γ ray in the positive-parity sequence, or the 420.7-keV transition in the negative-parity structure. The placement of the 76.5-keV transition is consistent with the observation of several low-energy ($\approx$100 keV) $E2$ transitions between the 12^+ and 10^+ states in neutron-rich Pt and Hg isotopes [2,5,23,24]. The total intensity of the unobserved 76.5-keV transition is determined using intensity balance considerations, and the γ intensity (Table I) is obtained considering the conversion coefficient [25] expected for a transition with $E2$ character. Note that the $(7^+) \rightarrow 5^+$, 699.0-keV transition is also newly identified.

TABLE I. Energies and intensities of γ rays, and energies and spins of initial and final levels in ^{196}Pt. DCO ratios are also presented when available. Transition energies are accurate to within 0.5 keV. Statistical errors on γ-ray intensities and DCO ratios are listed.

E_γ (keV)	E_i (keV)	→	E_f (keV)	I_i^π	→	I_f^π	I_γ	DCO ratio
(76.5)	2722	→	2646	(12^+)	→	(10^+)	0.83(5)	
103.0	1372	→	1269	7^-	→	5^-	7.0(2)	
149.0	4135	→	3986	(20^+)	→	(18^+)	2.1(1)	
151.0	3038	→	2887	–	→	(12^-)	2.1(1)	
163.5	5241	→	5077	(26^+)	→	(24^+)	0.99(8)	
256.0	2722	→	2466	(12^+)	→	11^-	1.5(1)	
326.0	1014	→	688	3^+	→	2^+	8.0(6)	
332.7	688	→	355	2^+	→	2^+	12.5(3)	
342.1	3986	→	3644	(18^+)	→	(16^+)	6.2(2)	0.98(12)
355.3	355	→	0	2^+	→	0^+	100.0(15)	
366.0	5077	→	4711	(24^+)	→	(22^+)	1.8(1)	
370.0	3092	→	2722	(14^+)	→	(12^+)	10.8(3)	0.95(7)
377.5	3416	→	3038	–	→	–	2.5(2)	
393.0	1269	→	876	5^-	→	4^+	61.8(19)	0.60(2)
393.5	2646	→	2252	10^+	→	8^+	17.8(5)	0.86(5)
409.0	1678	→	1269	6^-	→	5^-	3.5(2)	
420.7	2887	→	2466	(12^-)	→	11^-	8.0(3)	0.60(4)
446.7	1819	→	1372	9^-	→	7^-	27.8(6)	0.85(5)
515.0	2415	→	1900	(10^-)	→	8^-	2.4(2)	
521.0	876	→	355	4^+	→	2^+	87.5(12)	1.01(4)
521.0	1535	→	1014	4^+	→	3^+	2.4(2)	
527.6	1900	→	1372	8^-	→	7^-	7.0(3)	
551.3	3644	→	3092	(16^+)	→	(14^+)	8.9(3)	0.85(8)
576.5	4711	→	4135	(22^+)	→	(20^+)	2.0(2)	
594.1	1608	→	1014	5^+	→	3^+	4.2(4)	
604.4	1292	→	688	4^+	→	2^+	4.9(5)	
647.3	2466	→	1819	11^-	→	9^-	14.4(4)	1.04(5)
648.8	1525	→	876	6^+	→	4^+	24.8(8)	
699.0	2307	→	1608	(7^+)	→	5^+	1.2(1)	
714.5	2007	→	1292	6^+	→	4^+	0.68(7)	
727.2	2252	→	1525	8^+	→	6^+	20.6(5)	1.14(8)

Some transitions in the negative-parity sequence are also placed for the first time (Fig. 1), beyond the ones established from the β^- decay of ^{196}Ir [26]. The transitions in this sequence are illustrated in Figs. 2(c) and (d), where the newly observed transitions are visible.

DCO ratios for transitions up to spin 18^+ in the positive-parity band are determined, and are assigned quadrupole character (Table I). Due to the paucity of statistics, DCO ratios

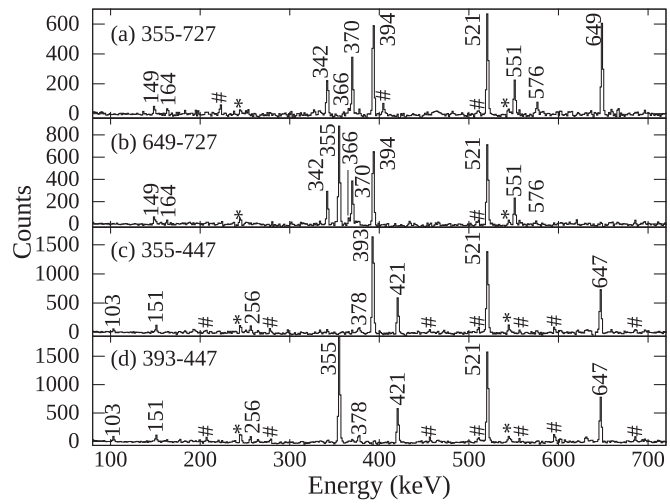

FIG. 2. Triple-γ coincidence spectra displaying transitions in the (a), (b) positive- and (c), (d) negative-parity sequences of ^{196}Pt. Asterisks indicate γ rays observed through coincidence with complementary multinucleon transfer products, while contaminant transitions are labeled with hash marks.

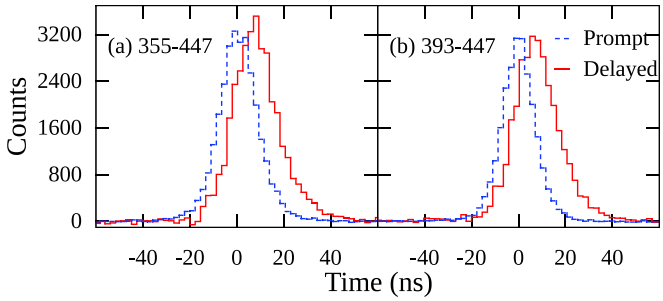

FIG. 3. (Color online) Effective half-life, 5.4(4) ns, for the closely spaced 5^- and 7^- levels. The time difference between the 446.7-keV γ ray above the 7^- state, and various transitions below the 5^- level, is indicated by the solid (red) line. The dotted line displays the time difference characteristic of prompt transitions with similar energies, for comparison.

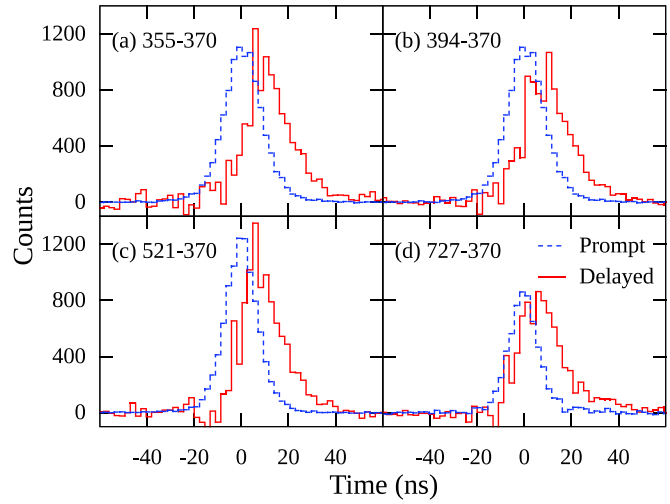

FIG. 4. (Color online) Time difference spectra illustrating the determination of the lifetime of the 12^+ state, in a manner similar to that in Fig. 3. A half-life of 7.7(7) ns is inferred from the observed centroid shift.

for transitions above the 18^+ state could not be established. The spin-parity assignments above spin $12\hbar$ in the positive-parity, yrast structure (Fig. 1) are marked as tentative since the 76.5-keV transition is not directly observed, and because the DCO ratio for the 256-keV γ ray could not be obtained. Tentative quadrupole character for transitions at the highest spin is supported by the observation of a single cascade with no appreciable branching to or from other states, and the absence of crossover $E2$ transitions which might have been observed if more than one transition in the sequence was of dipole character. In the negative-parity sequence, the DCO ratios for the 647.3- and 420.7-keV transitions indicate quadrupole and dipole nature, respectively, leading to the proposed spin-parity assignments. The multipolarity of the 151- and 377.5-keV transitions at the top of this sequence could not be determined.

The 5^- and 7^- states in the negative-parity sequence of ^{196}Pt had previously been determined to be isomeric, with half-lives of 1.1(2) ns and 5.2(2) ns, respectively. This is consistent with the observation of similar isomers in neighboring even-Pt isotopes [5]. In the present experiment, decreased statistics for the 7^- to 5^-, 103-keV transition prevented determination of distinct lifetimes for the two states. However, it was possible to extract an effective lifetime (for these 5^- and 7^- states) utilizing the technique described in section II. The measured effective half-life is 5.4(4) ns, in agreement with the value expected from the adopted values of the 5^- and 7^- half-lives. The effective half-life has been determined from the observed centroid shift of the time difference between the 355.3- and 446.7-keV, and 393- and 446.7-keV γ rays (below and above the 5^- and 7^- states, respectively), as compared to two prompt transitions with similar energies (Fig. 3).

The 12^+ isomeric state established in other even-Pt isotopes [5] was not known in ^{196}Pt. All transitions above the 12^+ state are observed in prompt coincidence, but those below this level show evidence for delayed feeding. As was the case with the negative-parity states, the time difference spectra for various pairs of transitions below and above the 12^+ state were examined. The shift in centroid, as compared to prompt transitions with similar energies (Fig. 4), implies $T_{1/2} = 7.7(7)$ ns. This half-life is associated here with the 12^+ state in a manner similar to what has been observed in the lighter, even-Pt isotopes. Based on the observed delayed feeding from the 12^+ state to the negative-parity sequence (through the 256-keV transition), it is unlikely that the 10^+ state is separately isomeric. Such an isomeric character is also not apparent for the 10^+ states in the lighter Pt isotopes [5,8], unlike the ones in Hg nuclei [27], where the $10^+ \rightarrow 8^+$ transitions have low energies ($\leqslant$100 keV) in comparison to a few hundred keV in the Pt case.

IV. DISCUSSION

A. Systematics of 7^- and 12^+ isomers in even Pt isotopes

The Pt isotopes exhibit evidence of prolate-oblate shape competition at relatively moderate spin with increase in neutron number from the proton-rich to neutron-rich region. In even-Pt nuclei ranging from $^{192-198}$Pt (Fig. 5), the 12^+ state has been found to be isomeric. The $\nu(i_{13/2})^2$ configuration is the only possible one able to provide the required $12\hbar$ of angular momentum. Confirmation of this configuration assignment is based on the measured negative g factor (≈ -0.17 for ^{190,192,194}Pt) [8]. The excitation energies of the 12^+ states exhibit a steady decrease, while the half-lives show a gradual increase, moving from the proton-rich Pt region to ^{194}Pt. This trend is related to the systematic lowering of the rotation-aligned states with increasing neutron number. A detailed discussion of this property is presented elsewhere [16]. The high excitation energy for the 12^+ state in ^{198}Pt ($N = 120$) is linked to the neutron Fermi level reaching the top of the $i_{13/2}$ subshell, and to the presence of a significant energy gap in the single-particle spectrum for larger N values. As a result, more energy is required to excite the valence $i_{13/2}$ neutron pair [16].

The yrast 10^+ states in heavier Pt isotopes are identified with a rotation-aligned oblate configuration, with the ground band 10^+ member being considerably higher in energy [5,8]. Further, a high-K, 10^+ assignment is ruled out based on the available valence orbitals. For the 10^+ states in Pt and Hg

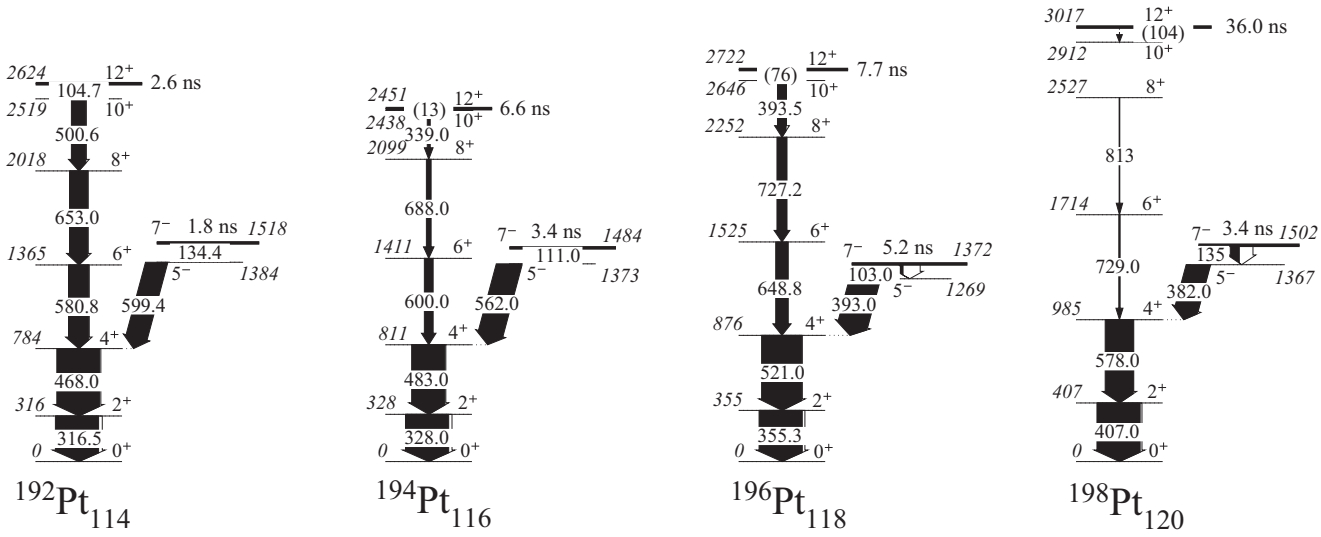

FIG. 5. Systematic comparison of the excited level structures de-exciting isomeric states in even-Pt isotopes from $^{192-198}$Pt [5,9,39]. Details are given in the text.

isotopes, both $(\nu i_{13/2})^2$ and $(\pi h_{11/2})^2$ assignments are possible. Experimental g factors favor $(\nu i_{13/2})^2$ character for the yrast 10^+ states in Hg isotopes [8]. The 10^+ states are also isomeric in several Hg isotopes [27] due to the relatively small $10^+ \rightarrow 8^+$ transition energy, as compared to Pt isotopes, owing to the lower moment-of-inertia of the ground-state bands in the former instance. The two-quasineutron assignment for the yrast 10^+ states is also supported by calculations which indicate that these are expected to be lower in energy compared to the two-quasiproton configuration in both Hg and Pt isotopes. A comparison of the yrast 10^+ and 12^+ energies in Pt and Hg isotopes ($N = 114$–120) reveal a very similar trend. Finally, the observed large variation (≈500 keV) in the yrast 10^+ energy from $N = 114$ to $N = 120$ argues against the two-quasiproton assignment. A conclusive determination of these configurations would require measurements of g factors of the 10^+ states across the Pt isotopic chain.

The 7^- isomers have been associated with a semidecoupled, two-quasiparticle structure [28] with varying degree of contributions from two-quasiproton $\pi^2(h_{11/2}, d_{3/2}/s_{1/2})$ and two-quasineutron $\nu^2(i_{13/2}, f_{5/2}/p_{3/2})$ configurations, involving nucleons in both high-j and low-j states [8,16]. In

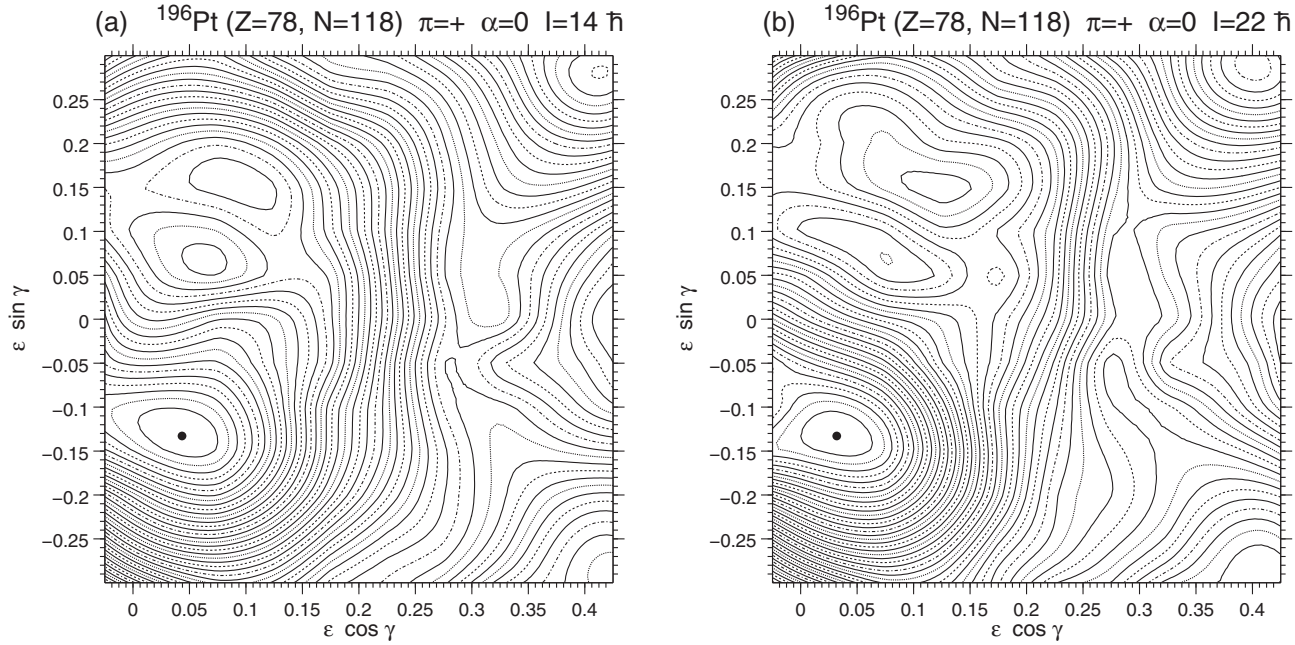

FIG. 6. Total energy surface plots illustrating energy minima in the positive-parity, yrast structure in ^{196}Pt, for different values of spin, from calculations performed using the UC code [32]. It is evident that the lowest energy minimum is oblate ($\gamma \approx -75^\circ$) at high spin: $I = 14\hbar$ and $I = 22\hbar$. The spacing between adjacent energy contours is 250 keV.

^{196}Pt, the measured value of the g factor ($= -0.03$) [29] underlines the dominance of the two-quasineutron component. The observation in ^{196}Pt of the 256-keV transition between the 12^+, $(\nu i_{13/2})^2$ state and the structure built on the 7^- level can be understood in terms of the common $i_{13/2}$ quasineutron.

The reduced $E2$ transition probability (in e^2b^2) can be expressed as

$$B(E2) = \frac{0.08156 B_\gamma}{E_\gamma^5 \tau [1 + \alpha_t(E2)]}, \quad (2)$$

where τ is the mean life of the level, α_t the total internal conversion coefficient, and B_γ represents the ratio of the intensity of the $E2$ γ ray to the total γ intensity of all transitions from the level [30]. In ^{196}Pt, the $B(E2)$ probability for the $12^+ \rightarrow 10^+$ transition is determined to be 0.16(3) e^2b^2 or 23(4) Weisskopf units, a definite indicator of the collective nature of the 12^+ isomeric state. Its magnitude is comparable (≈ 0.6 times) to that reported for the $2^+ \rightarrow 0^+$ transition in ^{196}Pt: $B(E2) = 0.275(1)$ e^2b^2 [31].

B. Cranked shell-model calculations

Cranking calculations have been performed to (i) understand shape evolution with spin in ^{196}Pt, and to (ii) investigate the possible role of both proton and neutron band crossings in generating high angular momentum. The ULTIMATE CRANKER (UC) code [32], incorporating the modified oscillator potential, and the cranking code with a Woods-Saxon (WS) potential with the universal parametrization [33] were used for two sets of calculations. For both, the proton and neutron pair-gap energies were obtained from experimental masses following the procedure described in Refs. [34,35]. The results from UC and WS calculations are presented below in terms of corresponding deformation parameters ϵ_2, ϵ_4 and β_2, β_4, respectively. The β and ϵ deformation parameters are similar for lower-order, small deformations, and to the first order are related through [36]

$$\epsilon_2 = \frac{3}{2}\left(\frac{5}{4\pi}\right)^{1/2} \beta_2 \approx 0.95\beta_2, \quad (3)$$

$$\epsilon_4 = -\left(\frac{9}{4\pi}\right)^{1/2} \beta_4 \approx -0.85\beta_4 \quad (4)$$

for quadrupole and hexadecapole deformations, respectively. The two parametrizations become considerably different for large deformations. The total energy surface plots from UC calculations and the quasiparticle levels from WS ones are presented to emphasize the qualitative agreement between the two approaches in terms of various predictions.

1. *Shape evolution in* ^{196}Pt

Representative total energy surface plots for the positive-parity, yrast structure in ^{196}Pt are displayed in Fig. 6. For $I = 10\hbar$ and beyond, an oblate energy minimum corresponding to $\epsilon_2 = 0.14$, $\gamma \approx -75^\circ$ deformation parameters becomes favored in energy. The energy surface plots for $I = 14\hbar$ and $I = 22\hbar$ are displayed in Fig. 6. It is evident that the oblate minimum persists well beyond $20\hbar$. It may be noted

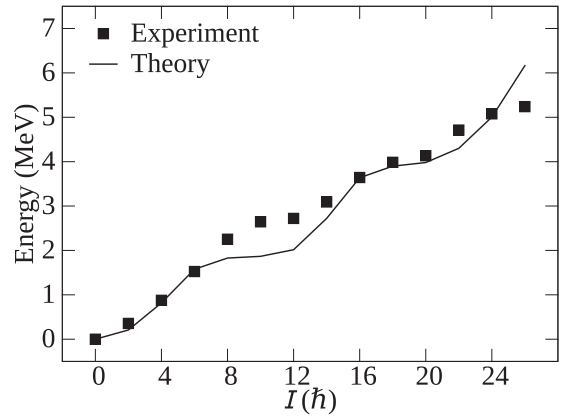

FIG. 7. Comparison of the experimental and calculated level energies for the positive-parity sequence in ^{196}Pt.

that the stability of the oblate minimum at high spin has been verified by employing an extended grid in deformation space to be sensitive to the appearance of possible energy minima well beyond $\gamma = -75^\circ$. Excitation energies for the

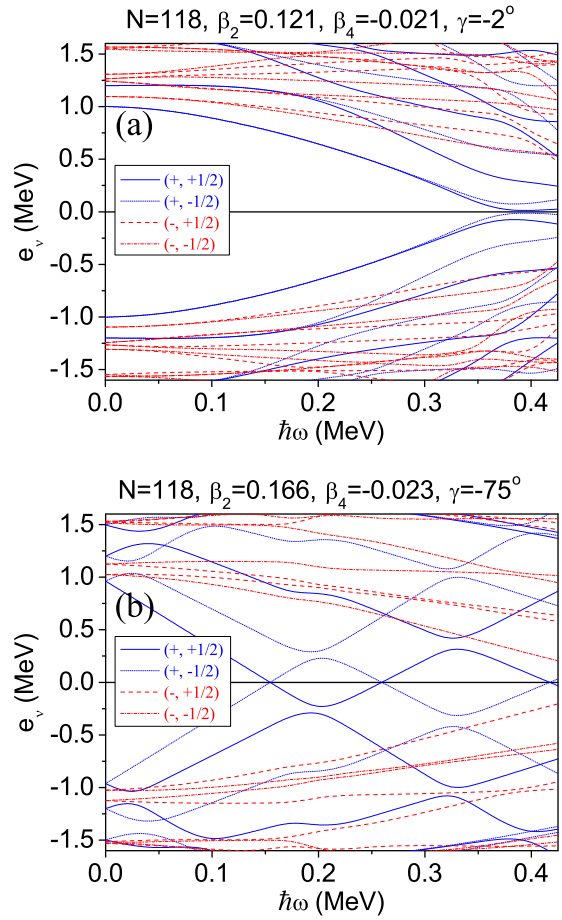

FIG. 8. (Color online) Neutron quasiparticle levels in ^{196}Pt calculated using the universal parametrization of the Woods-Saxon potential for (a) prolate and (b) oblate deformations. The deformation parameters are indicated.

yrast, positive-parity states have also been determined from the calculations. They are compared with those observed in Fig. 7. The discontinuities present in the data around $I = 10\hbar$ and $I = 18\hbar$, arise from the rotation alignment of nucleons, and are reproduced by the calculations, although the excitation energy near $I = 10\hbar$ is underpredicted by ∼0.5 MeV. Overall, the calculations are in reasonable agreement with the data.

2. *Rotation alignments for Pt isotopes at prolate and oblate deformations*

In the $A \approx 180$–190 region, most proton-rich nuclei are prolate near the ground state. For proton-rich isotopes, low-Ω orbitals of the $i_{13/2}$ subshell are occupied. With increasing rotational frequency, $i_{13/2}$ neutrons are expected to first undergo rotation alignment, while $h_{11/2}$ protons are predicted to align at significantly higher frequencies. As the neutron number increases along an isotopic chain, the neutron alignment frequency (for prolate deformation) is expected to increase as successively higher-Ω orbitals become occupied. Conversely, for oblate shapes, the Ω value in the $i_{13/2}$ subshell decreases for higher neutron numbers, and the band crossing should occur at a lower rotational frequency. Oblate, rotation-aligned structures with moments of inertia

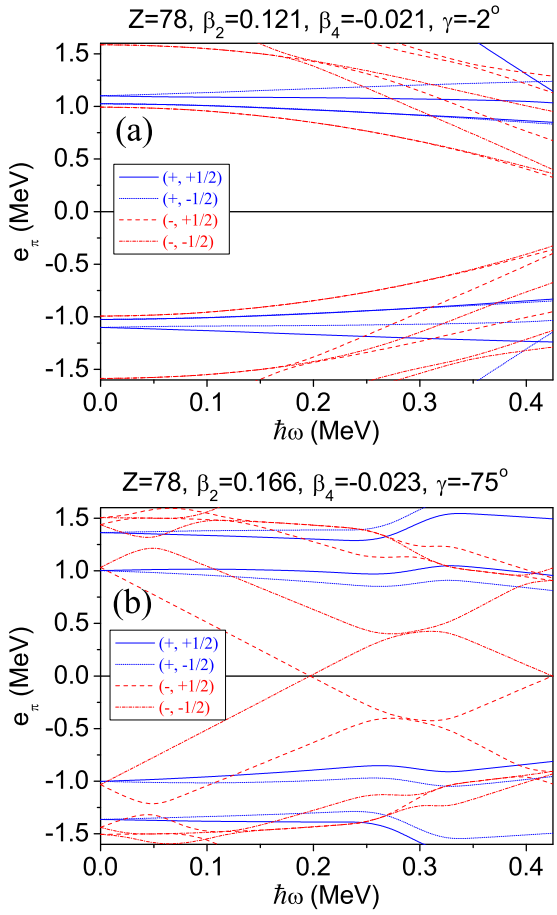

FIG. 9. (Color online) Proton quasiparticle levels in ^{196}Pt calculated in a similar manner as in Fig. 8: for (a) prolate and (b) oblate deformations.

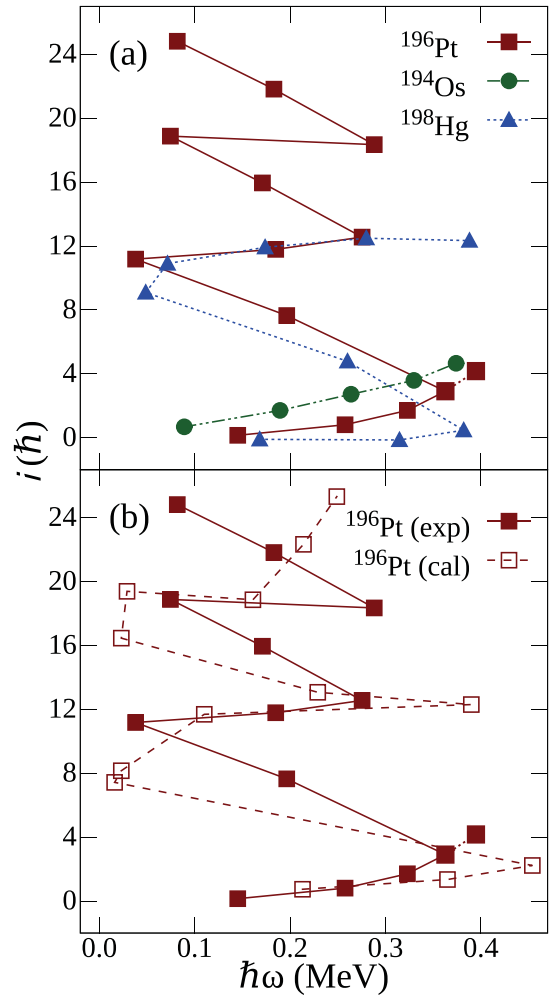

FIG. 10. (Color online) (a) Aligned angular momentum as a function of rotational frequency for $N = 118$ isotones ^{196}Pt ($Z = 78$), ^{194}Os ($Z = 76$) [38], and ^{198}Hg ($Z = 80$) [24]. A reference rotor with $J_0 = 8\ \hbar^2\text{MeV}^{-1}$ and $J_1 = 35\ \hbar^4\text{MeV}^{-3}$, appropriate for a comparison of the three isotones, is used. (b) Comparison of experimental and calculated aligned angular momentum for the yrast, positive-parity sequence in ^{196}Pt. Satisfactory agreement is evident between the crossing frequencies and magnitude of aligned angular momentum for the first two alignments.

considerably higher than those associated with the prolate ground-state band are, therefore, realized at lower rotational frequencies as N increases and become the favored excitation mode at high spin.

The neutron quasiparticle levels in ^{196}Pt, calculated as a function of rotational frequency both for prolate and oblate shapes, can be found in Figs. 8(a) and (b), while the ones for protons are displayed in Figs. 9(a) and (b) for the same deformation parameters. These Routhians provide a good illustration of the higher band crossing frequency ($\hbar\omega = 0.38$ MeV) for neutrons in the $\Omega = 11/2$ component of the $i_{13/2}$ subshell at prolate deformation [Fig. 8 (a)], when compared to $\hbar\omega = 0.23$ MeV for $\Omega = 3/2$ neutrons in the same subshell, but for an oblate shape. Figure 10 illustrates the aligned angular

momentum for the positive-parity sequence in ^{196}Pt, with a backbend evident around 0.2 MeV, in accordance with the calculations for an oblate shape. A possible, small up bend in the ground state band (data point for ^{196}Pt connected by a dashed line in Fig. 10) is visible if the 10^+ state tentatively identified earlier [10] is included. The first neutron alignment has *AB* character [37], while the *CD* alignment is expected to occur at higher frequency. In the case of protons, a similar situation is evident for low- and high-Ω components of the $h_{11/2}$ subshell. The *ab* crossing frequency for an oblate shape is $\hbar\omega \approx 0.3$ MeV [Fig. 9 (b)], much lower than that calculated for prolate deformation [Fig. 9 (a)]. The reinforcing effect of both neutron and proton alignments at lower rotational frequencies strongly favors oblate shapes at high spin. The gain in aligned angular momentum (Fig. 10) at the first backbend in ^{196}Pt is $\sim 11\hbar$, i.e., close to the $12\hbar$ expected from the full alignment of an $i_{13/2}$ neutron pair. Second and third alignments are visible at similar frequencies for higher spin. The gain in aligned angular momentum due to the second alignment is $\sim 8\hbar$ (Fig. 10). For *CD* neutron and *ab* proton crossings, alignment gains of $8\hbar$ and $10\hbar$, respectively, are indicated by the calculations. Therefore, it is likely that the second alignment is associated with the *CD* neutron crossing. The calculated frequencies for the second and third crossings are higher than the experimental values (Figs. 8, 9, 10). Lower crossing frequencies would be consistent with a smaller magnitude of oblate deformation (β_2) than that obtained from calculations and/or with reduced pairing in the aligned states. Only the first alignment is visible in the $N = 118$ isotone ^{198}Hg, where states up to $20\hbar$ are established [16,24], while in ^{194}Os, information is limited up to $10\hbar$ in the prolate structure [38].

V. SUMMARY

A rotation-aligned, isomeric state with $I^\pi = 12^+$, and a $(\nu i_{13/2})^2$ configuration, was established in ^{196}Pt, and a half-life of 7.7(7) ns was measured. The reduced $E2$ transition probability for the de-excitation of this isomer supports its assignment as a collective state. A positive-parity sequence built on this state is identified up to high spin, and is associated with collective oblate rotation, including a large contribution from aligned angular momentum. A discontinuous increase in aligned angular momentum, due to possible $i_{13/2}$ neutron and $h_{11/2}$ proton alignments is visible in the oblate sequence. Cranking calculations provide a good account of the experimental observables and indicate that an oblate shape is strongly favored at high spin.

ACKNOWLEDGMENTS

We would like to thank I. Ahmad, J. P. Greene, A. J. Knox, D. Peterson, U. Shirwadkar, X. Wang, and C. M. Wilson for assistance during the experiment. S.G.W. acknowledges support from the INSPIRE PhD Fellowship of the Department of Science and Technology, Government of India (Fellowship No. IF150098). S.K.T. would like to acknowledge support from the Board of Research in Nuclear Sciences, India, and the University Grants Commission, India. This work is supported by the U.S. Department of Energy, Office of Science, Office of Nuclear Physics, under Award Nos. DE-FG02-94ER40848 and DE-FG02-94ER40834, and Contract No. DE-AC02-06CH11357. The research described here utilized resources of the ATLAS facility at ANL, which is a DOE Office of Science user facility.

[1] R. R. Hilton and H. J. Mang, Phys. Rev. Lett. **43**, 1979 (1979).
[2] M. Piiparinen, J. C. Cunnane, P. J. Daly, C. L. Dors, F. M. Bernthal, and T. L. Khoo, Phys. Rev. Lett. **34**, 1110 (1975).
[3] U. S. Tandel, S. K. Tandel, P. Chowdhury, D. Cline, C. Y. Wu, M. P. Carpenter, R. V. F. Janssens, T. L. Khoo, T. Lauritsen, C. J. Lister, D. Seweryniak, and S. Zhu, Phys. Rev. Lett. **101**, 182503 (2008).
[4] G. D. Dracoulis, G. J. Lane, A. P. Byrne, H. Watanabe, R. O. Hughes, F. G. Kondev, M. Carpenter, R. V. F. Janssens, T. Lauritsen, C. J. Lister, D. Seweryniak, S. Zhu, P. Chowdhury, Y. Shi, and F. R. Xu, Phys. Lett. B **720**, 330 (2013).
[5] S. A. Hjorth, A. Johnson, Th. Lindblad, L. Funke, P. Kemnitz, and G. Winter, Nucl. Phys. A **262**, 328 (1976).
[6] M. Caamano, P. M. Walker, P. H. Regan, M. Pfutzner, Zs. Podolyak, J. Gerl, M. Hellstrom, P. Mayet, M. N. Mineva, A. Aprahamian *et al.*, Eur. Phys. J. A **23**, 201 (2005).
[7] S. J. Steer, Zs. Podolyak, S. Pietri, M. Gorska, H. Grawe, K. H. Maier, P. H. Regan, D. Rudolph, A. B. Garnsworthy, R. Hoischen *et al.*, Phys. Rev. C **84**, 044313 (2011).
[8] A. I. Levon, Yu. V. Nosenko, V. A. Onischuk, A. A. Schevchuk, and A. E. Stuchbery, Nucl. Phys. A **764**, 24 (2006).
[9] G. A. Jones, Zs. Podolyak, N. Schunck, P. M. Walker, G. De Angelis, Y. H. Zhang, M. Axiotis, D. Bazzacco, P. G. Bizzeti, F. Brandolini *et al.*, Acta. Phys. Pol. B **36**, 1323 (2005).
[10] A. Mauthofer, K. Stelzer, J. Idzko, Th. W. Elze, H. J. Wollersheim, H. Emling, P. Fuchs, E. Grosse, and D. Schwalm, Zeitschrift fur Physik A **336**, 263 (1990).
[11] D. Cline, Annu. Rev. Nucl. Part. Sci. **36**, 683 (1986).
[12] C. Y. Wu, D. Cline, T. Czosnyka, A. Backlin, C. Baktash, R. M. Diamond, G. D. Dracoulis, L. Hasselgren, H. Kluge, B. Kotlinski, J. R. Leigh, J. O. Newton, W. R. Phillips, S. H. Sie, J. Srebrny, and F. S. Stephens, Nucl. Phys. A **607**, 178 (1996).
[13] C. S. Lim, R. H. Spear, M. P. Fewell, and G. J. Gyapong, Nucl. Phys. A **548**, 308 (1992).
[14] J. E. Garcia-Ramos, K. Heyde, L. M. Robledo, and R. Rodriguez-Guzman, Phys. Rev. C **89**, 034313 (2014).
[15] J. M. Allmond, J. L. Wood, and W. D. Kulp, Phys. Rev. C **81**, 051305(R) (2010).
[16] S. K. Tandel, S. G. Wahid, P. Chowdhury, R. V. F. Janssens, M. P. Carpenter, T. L. Khoo, F. G. Kondev, T. Lauritsen, C. J. Lister, D. Seweryniak, and S. Zhu, Phys. Lett. B **750**, 225 (2015).
[17] I-Yang Lee, Nucl. Phys. A **520**, 641c (1990).
[18] R. V. F. Janssens and F. S. Stephens, Nucl. Phys. News **6**, 9 (1996).
[19] D. C. Radford, Nucl. Instrum. Methods Phys. Res. A **361**, 297 (1995).

[20] K. S. Krane, R. M. Steffen, and R. M. Wheeler, Nucl. Data Tables **11**, 351 (1973).
[21] A. Kramer-Flecken, T. Morek, R. M. Lieder, W. Gast, G. Hebbinghaus, H. M. Jager, and W. Urban, Nucl. Instrum. Methods Phys. Res. A **275**, 333 (1989).
[22] H.-Q. Jin, TSCAN and related programs. A package to perform tape scanning and to manipulate matrices, RUTGERS-ORNL-UTK, 1992–1997.
[23] H. Helppi, S. K. Saha, P. J. Daly, S. R. Faber, and T. L. Khoo, Phys. Rev. C **28**, 1382 (1983).
[24] C. Gunther, H. Hubel, A. Kleinrahm, D. Mertin, B. Richter, W. D. Schneider, and R. Tischler, Phys. Rev. C **15**, 1298 (1977).
[25] T. Kibedi, T. W. Burrows, M. B. Trzhaskovskaya, P. M. Davidson, C. W. Nestor, Jr., Nucl. Instrum. Methods Phys. Res. A **589**, 202 (2008).
[26] J. F. W. Jansen, H. Pauw, and C. J. Toese, Nucl. Phys. A **115**, 321 (1968).
[27] M. Guttormsen, A. Von Grumbkow, Y. K. Agarwal, K. P. Blume, K. Hardt, H. Hubel, J. Recht, P. Schuler, H. Kluge, K. H. Maier, A. Maj, and N. Roy, Nucl. Phys. A **398**, 119 (1983).
[28] K. Neergard, P. Vogel, and M. Radomski, Nucl. Phys. A **238**, 199 (1975).
[29] B. I. Gorbachev, A. I. Levon, O. F. Nemets and O. B. Sevastyuk, Program and Theses, Proceedings of the 33rd Annual Conference on Nuclear Spectroscopy and the Structure of the Atomic Nucleus, Moscow, p. 147 (1983) (unpublished).
[30] H. Ejiri and M. J. A. de Voigt, *Gamma-Ray and Electron Spectroscopy in Nuclear Physics* (Clarendon, Oxford, 1989), Chap. 6.
[31] H. H. Bolotin, A. E. Stuchbery, I. Morrison, D. L. Kennedy, and C. G. Ryan, Nucl. Phys. A **370**, 146 (1981).
[32] T. Bengtsson, Nucl. Phys. A **512**, 124 (1990).
[33] S. Ćwiok, J. Dudek, W. Nazarewicz, J. Skalski, and T. Werner, Comp. Phys. Comm. **46**, 379 (1987).
[34] Peter Moller, Arnold J. Sierk, Ragnar Bengtsson, Hiroyuki Sagawa, and Takatoshi Ichikawa, Phys. Rev. Lett. **103**, 212501 (2009).
[35] S. K. Tandel, P. Chowdhury, E. H. Seabury, I. Ahmad, M. P. Carpenter, S. M. Fischer, R. V. F. Janssens, T. L. Khoo, T. Lauritsen, C. J. Lister, D. Seweryniak, and Y. R. Shimizu, Phys. Rev. C **73**, 044306 (2006).
[36] Sven Gösta Nilsson and Ingemar Ragnarsson, *Shapes and Shells in Nuclear Structure* (Cambridge University Press, Cambridge, 1995), Chap. 8, pp. 121–126.
[37] R. Bengtsson, S. Frauendorf, and F. R. May, At. Data Nucl. Data Tables **35**, 15 (1986).
[38] C. Wheldon, J. Garces Narro, C. J. Pearson, P. H. Regan, Zs. Podolyak, D. D. Warner, P. Fallon, A. O. Macchiavelli, and M. Cromaz, Phys. Rev. C **63**, 011304(R) (2000).
[39] C. Wheldon, http://www.nndc.bnl.gov/xundl.